

Papers published in *Hydrology and Earth System Sciences Discussions* are under open-access review for the journal *Hydrology and Earth System Sciences*

HTESSEL evaluation

E. L. Wipfler et al.

Seasonal evaluation of the land surface scheme HTESSEL against remote sensing derived energy fluxes of the Transdanubian region in Hungary

E. L. Wipfler¹, K. Metselaar¹, J. C. van Dam¹, R. A. Feddes¹, E. van Meijgaard², L. H. van Ulft², B. van den Hurk^{2,3}, S. J. Zwart^{4,5}, and W. G. M. Bastiaanssen^{4,5}

¹Wageningen University, Soil Physics, Ecohydrology and Groundwater Management Group, Wageningen, The Netherlands

²Royal Netherlands Meteorological Institute, the Bilt, The Netherlands

³Institute for Marine and Atmospheric Research, Utrecht, The Netherlands

⁴WaterWatch, Wageningen, The Netherlands

⁵Delft University of Technology, Department of Water Management, Delft, The Netherlands

Received: 30 July 2009 – Accepted: 6 September 2009 – Published: 8 October 2009

Correspondence to: E. L. Wipfler (louise.wipfler@wur.nl)

Published by Copernicus Publications on behalf of the European Geosciences Union.

Title Page

Abstract

Introduction

Conclusions

References

Tables

Figures

◀

▶

◀

▶

Back

Close

Full Screen / Esc

Printer-friendly Version

Interactive Discussion



Abstract

The skill of the land surface model HTESSSEL is assessed to reproduce evaporation in response to land surface characteristics and atmospheric forcing, both being spatially variable. Evaporation estimates for the 2005 growing season were obtained from satellite observations of the Western part of Hungary and compared to model outcomes. Atmospheric forcing was obtained from a hindcast run with the Regional Climate Model RACMO. Although HTESSSEL slightly underestimated the seasonal evaporative fraction, the mean, 10th and 90th percentile of this variable were of the same magnitude as the satellite observations. The initial water as stored in the soil and snow layer did not have a significant effect on the statistical properties of the evaporative fraction. However, the spatial distribution of the initial soil and snow water affected significantly the spatial distribution of the calculated evaporative fraction and the models ability to reproduce evaporation correctly in low precipitation areas in the considered region. HTESSSELs performance appears to be less in dryer areas. In Western Hungary these areas are situated in the Danube valley, which is partly covered by irrigated cropland and which also may be affected by shallow groundwater. Incorporating (lateral) groundwater flow and irrigation, processes that are not included now, may improve HTESSSELs ability to predict evaporation correctly. Evaluation of the model skills using other test areas and larger evaluation periods is needed to confirm the results.

Based on earlier sensitivity analysis, the effect of a number of modifications to HTESSSEL was assessed. A more physically based reduction function for dry soils was introduced, the soil depth was made variable and the effect of swallow groundwater included. However, the modification did not lead to significant improved performance of HTESSSEL.

HESSD

6, 6293–6334, 2009

HTESSSEL evaluation

E. L. Wipfler et al.

[Title Page](#)

[Abstract](#)

[Introduction](#)

[Conclusions](#)

[References](#)

[Tables](#)

[Figures](#)



[Back](#)

[Close](#)

[Full Screen / Esc](#)

[Printer-friendly Version](#)

[Interactive Discussion](#)



1 Introduction

A problem often reported in climate simulations is a systematic summer drying that results in too dry and too warm projections of summertime climate in southeastern Europe (Hagemann et al., 2004). This summer drying is associated with a strong reduction of the hydrological cycle, dry soils, strong soil evaporation and plant transpiration stress and reduced precipitation. These models often overemphasize the positive feedback between precipitation and the vapor flux due to soil evaporation and plant transpiration¹ (e.g. Betts et al., 1996; Lenderink et al., 2003; Hagemann et al., 2004). Presumably, land surface processes play an important role in this feedback (Fischer et al., 2007). Improving the representation of the soil hydrological processes may impact the precipitation-evaporation feedback. Using the land surface scheme TESSEL (Tiled ECMWF Scheme for Surface Exchange over Land; Van den Hurk et al., 2000), Lenderink et al. (2003) pragmatically solved the tendency of a summer continental dry bias in their *Regional Climate Model* (RCM) by increasing the soil reservoir depth of TESSEL and applying a non-linear dependency of canopy resistance on available soil water. It is unclear how realistic these modifications are, and whether their application is still valid when extrapolating to changing climate conditions.

A new version of TESSEL has been developed (*Hydrology-TESEL*; Balsamo et al., 2009), that appears to improve the skill of the ECMWF Integrated Forecast System to forecast the 2003 European heatwave (Weisheimer, personal communication). A thorough test with station data and area integrated atmospheric moisture budgets (i.e. runoff data and atmospheric water balance data by Hirschi et al., 2006; Seneviratne et al., 2004) confirmed the general improvement of HTESEL over its predecessor (Balsamo et al., 2009). To assess the behavior of a land surface model like HTESEL in the hydrological feedback cycle, however, a systematic evaluation of land surface evaporation at a regional scale is deemed necessary. Such an evaluation has been

¹In the following, the combined vapor flux of soil evaporation and plant transpiration will be referred to as evaporation or evaporative flux.

[Title Page](#)

[Abstract](#)

[Introduction](#)

[Conclusions](#)

[References](#)

[Tables](#)

[Figures](#)



[Back](#)

[Close](#)

[Full Screen / Esc](#)

[Printer-friendly Version](#)

[Interactive Discussion](#)



severely hampered by a lack of reliable and spatially explicit surface evaporation data.

To evaluate the spatial variability of seasonal mean surface evaporation from HTESSEL in a central European continental area in the Danube basin, the present study applies a spatial evaporation estimate for the 2005 growing season being derived from satellite observations. This area appears to be particularly prone to pronounced summer drying (Lenderink et al., 2003).

The primary objective is to assess the model skill in reproducing the spatial distribution of surface evaporation in response to the spatial distribution in precipitation and land surface characteristics. The secondary goal is to assess the effect of a number of HTESSEL model updates. Planned simulations with the land surface scheme implemented in a full 3-D regional atmospheric model will address the model's ability to reproduce the land-atmosphere feedback in this area, which is necessary for long-term weather and climate projection.

2 The land surface scheme HTESSEL

In the land surface scheme HTESSEL (ECMWF, 2007; Balsamo et al., 2009) for each grid cell of the atmospheric model the land surface is represented by 6 tiles over land (bare ground, low and high vegetation, intercepted water, shaded and exposed snow). For each tile separately the energy balance is calculated:

$$(1 - \alpha_i)R_s^\downarrow + R_l^\downarrow - R_l^\uparrow - G_i = H_i + \lambda E_i, \quad (1)$$

where R_s and R_l (W m^{-2}) are the flux densities of short wave and long wave radiation, respectively, with the arrows refer to incoming (\downarrow) and outgoing (\uparrow) flux densities, α_i is albedo, H_i , λE_i and G_i (W m^{-2}) denote the sensible, latent and soil heat flux density of tile i , respectively, λ (J kg^{-1}) the specific latent heat of vaporization and E ($\text{kg m}^{-2} \text{s}^{-1}$) the mass flux density of evaporation. Total H , G and λE are calculated as the area weighted average over the tiles. Soil heat is redistributed over a fixed vertical grid of 4

Title Page

Abstract

Introduction

Conclusions

References

Tables

Figures

◀

▶

◀

▶

Back

Close

Full Screen / Esc

Printer-friendly Version

Interactive Discussion



soil layers (extending to 2.89 m depth) using a standard diffusion scheme, allowing for thermal contributions from soil water freezing and melting (Viterbo et al., 1999).

Turbulent heat and water vapor fluxes from each tile are calculated using a resistance analogy, where an aerodynamic and surface resistance accounts for the transfer efficiency of heat or water vapor over a vertical temperature and humidity gradient. The surface resistance r_c is a function of R_s^\downarrow , leaf area index LAI ($\text{m}^2 \text{m}^{-2}$), average unfrozen soil water content θ ($\text{m}^3 \text{m}^{-3}$), atmospheric water deficit D_a (Pa), and minimum stomatal resistance $r_{s,\min}$ (s m^{-1}) (Jarvis, 1976):

$$r_c = \frac{r_{s,\min}}{\text{LAI}} f_1(R_s^\downarrow) f_2(\bar{\theta}) f_3(D_a). \quad (2)$$

In particular, the sensitivity of evaporation to soil water content is relevant to discuss here, as it affects the seasonal evolution of evaporation and soil water content, i.e.:

$$f_2^{-1} = \frac{\bar{\theta} - \theta_{\text{wp}}}{\theta_{\text{fc}} - \theta_{\text{wp}}}, \quad (3)$$

where θ_{wp} and θ_{fc} are the soil water contents at permanent wilting point and at field capacity, respectively, and $\bar{\theta}$ is the root density weighted average water content over all soil layers of the unfrozen soil water. Hence, when $\bar{\theta} < \theta_{\text{fc}}$ the resistance increases and becomes infinite at wilting point. Vertical root density distributions have been derived following Zeng et al. (1998) and adapted to a multilayer configuration. Coefficients for f_1 , f_2 and f_3 are taken from a lookup table, for which an externally prescribed vegetation type forms the entry. Vegetation data are derived from ECOCLIMAP (Masson et al., 2003).

The water balance (mm d^{-1}) at the land surface is described by:

$$\Delta W + \Delta S = P - E - R \quad (4)$$

where ΔW represents the change in water storage of the soil moisture and interception reservoir, ΔS the change in accumulated snowpack, P represents precipitation, E

Title Page

Abstract

Introduction

Conclusions

References

Tables

Figures

◀

▶

◀

▶

Back

Close

Full Screen / Esc

Printer-friendly Version

Interactive Discussion



represents evaporation of soil (E_{soil}), vegetation (E_{veg}) and intercepted water (E_i), R surface and subsurface runoff (see Fig. 1).

Initially, precipitation is collected in the interception reservoir until it is saturated. Then, excess precipitation is partitioned between surface runoff and infiltration into the soil column. When the imposed water flux exceeds the maximum possible soil infiltration rate, excess water is taken as surface runoff as described by the so-called Arno scheme, while accounting for sub-grid variability related to orography (Dümenil and Todini, 1992; Van den Hurk et al., 2002).

Soil water flow in HTESSSEL is described by the diffusivity form of the Richards' equation using the same four-layer discretization as for soil temperature (with increasing thickness from the soil surface downwards, i.e. 0.07, 0.21, 0.72 and 1.89 m). The dependencies of the soil hydraulic conductivity k (m s^{-1}) and soil water diffusivity D ($\text{m}^2 \text{s}^{-1}$) on θ are described by means of the analytical functions of Van Genuchten (1980). Hydraulic coefficients are specific for six soil textures, i.e. coarse, medium, medium-fine, fine, very fine and organic.

HTESSSEL does not account for either lateral exchange of soil water between the grid elements and/or irrigation. Excess water leaves the domain as either surface or subsurface runoff. At the bottom of the soil column, free drainage is assumed. Alternative lower boundary conditions are not considered.

3 Site and observations

3.1 Transdanubian test region

The test region covers the western region of Hungary between approx. 45.5–48.5° N and 16.0–20.0° E being the Transdanubian region. Most of the area is flat and bounded by the Alps in the southwest and the Tatra in the northwest. The climate of Hungary can be described as a typical European continental climate with warm, dry summers and fairly cold winters. Average precipitation, P is 612 mm yr^{-1} and the average annual

Title Page

Abstract

Introduction

Conclusions

References

Tables

Figures

◀

▶

◀

▶

Back

Close

Full Screen / Esc

Printer-friendly Version

Interactive Discussion



Title Page

Abstract

Introduction

Conclusions

References

Tables

Figures

◀

▶

◀

▶

Back

Close

Full Screen / Esc

Printer-friendly Version

Interactive Discussion



temperature at 2 m height, T_{a2m} is about 10°C. The average summer T_{a2m} is approximately 19.6°C and the average winter T_{a2m} is 0.4°C (Szalia et al., 2005). The soils in the area can be classified as acid and non-acid loamy, well-drained soils, salt affected, sodium rich and imperfectly drained soils (Dobris report, Soil map of Europe, 1995).

About 2/3 of the land is under cultivation. The remaining vegetation is mainly deciduous forest and mixed forest (Masson et al., 2003). In Fig. 2 the percentage of areas under irrigation is given for the area considered (Siebert et al., 2007), which reveals that especially along the Danube valley the percentage of irrigated land is up to 50%. The yearly amount of irrigated water associated with these figures is unknown, e.g. it depends on the type of crop, irrigation technique, climate and season.

Measurements taken at the two flux-towers from the CarboEuropeIP database (Tuba et al., 2005) being located in Matra and Bugac, were used as ground truth of the satellite observations. The Matra tower is located at 47° 50' 30" N and 19° 43' 33" E at 350 m a.s.l. and the tower in Bugac is located at 46° 41' 30" N and 19° 36' 06" E at 111 m a.s.l (see Fig. 2). Both towers are situated in a grassland ecosystem.

3.2 Areal precipitation using TRMM

Area covering space-born precipitation, P , is provided by the *Tropical Rainfall Measuring Mission* (TRMM) on a monthly basis at a resolution of 0.25°. Comparison of the space-born annual precipitation with the precipitation measured at 35 weather stations in the region shows that in 2005 TRMM appears to over-predict precipitation. This occurs especially in low precipitation areas, where differences could be up to 400 mm. Therefore, we corrected the TRMM precipitation using the linear regression relation between satellite and ground observations on an annual basis (see Fig. 3a). The corrected annual TRMM precipitation over the test area is given in Fig. 3b. The correlation coefficient of the corrected TRMM precipitation to the meteorological data is 0.73. Annual precipitation over 2005 was on average 652 mm. The highest annual precipitation (around 900 mm) was measured in the mountainous southwestern and northeastern part of the region. In the Danube valley including Lake Balaton, the annual precipitation

was low, down to 450 mm.

3.3 Energy fluxes from satellite images

3.3.1 SEBAL algorithm

The energy partitioning algorithm *Surface Energy Balance Algorithms for Land* (SEBAL, Bastiaanssen et al., 1998, 2005) estimates pixel wise latent heat fluxes using the surface energy balance (Eq. 1) with thermal and shortwave radiance information from satellite images and routine meteorological data (i.e. air temperature T_{a2m} ($^{\circ}\text{C}$), wind speed u (m s^{-1}) and relative humidity RH (–)).

In order to infer weekly estimates of the surface energy fluxes, the SEBAL algorithm was applied for 19 cloud-free images of the test region from the Terra and Aqua sensors onboard of the *MOderate Resolution Imaging Spectrometer* (MODIS) satellite. This satellite passes daily and the thermal bands, which are dominant in the SEBAL calculations, have a spatial resolution of 1 km. Meteorological data were obtained from 35 stations in Western Hungary and bordering countries and spatially interpolated by using an interpolation method that includes land use, vegetation density and elevation (Voogt, 2006).

Daily net radiation R_{n24} (W m^{-2}) was computed using satellite measured broadband surface albedo α , extraterrestrial solar radiation $R_{s,exo}^{\downarrow}$ (Wm^{-2}) and incoming short wave radiation (ground truth) R_s^{\downarrow} according to De Bruin and Stricker (2000):

$$R_{n24} = (1 - \alpha)R_s^{\downarrow} - 110R_s^{\downarrow}/R_{s,exo}^{\downarrow}. \quad (5)$$

Since R_s^{\downarrow} was not available from the 35 meteorological stations, R_s^{\downarrow} from the Bugac and Matra flux-towers was used instead. The measurements from the two towers have been averaged and used as input to the SEBAL calculations, hence ignoring spatial patterns of incoming radiation.

Title Page

Abstract

Introduction

Conclusions

References

Tables

Figures

◀

▶

◀

▶

Back

Close

Full Screen / Esc

Printer-friendly Version

Interactive Discussion



The soil heat flux density G was computed as a variable fraction of R_n , taking into account the presence of leaves by means of the *Normalized Difference Vegetation Index* (NDVI) and the surface temperature (warmer surfaces have higher G/R_n fractions).

The sensible heat flux density H was estimated following the standard Monin-Obukhov theorem for turbulent exchange processes and thermal convection. For this pixel wise forcing, air temperature, relative humidity and wind speed are required. Prior to the single pixel computation, extreme values of H were determined. An extreme wet pixel was identified based on the maps of surface temperature and the NDVI, and for these conditions it was assumed that $H=0$. Similarly, an extreme dry pixels was selected where H was set equal to R_n-G .

The weekly energy fluxes were obtained by re-applying the SEBAL algorithm with the average meteorological data for periods of which no surface observations could be retrieved due to cloud cover. The bio-physical parameters such as surface albedo, NDVI, emissivity, surface roughness and bulk surface resistance, were estimated at the time of cloud free satellite observations and assumed constant over the cloudy period.

3.3.2 Comparison of SEBAL obtained net radiation and evaporation with tower based data

For 19 cloud free observation days, daily averaged R_n and λE from SEBAL were compared with the R_n and λE from the towers Matra and Bugac. At both towers, λE was measured using eddy-correlation. At both Matra and Bugac, the daily energy balance did not close, i.e. the available energy (R_n+G) was larger than ($H+\lambda E$). The difference on a sunny day in June could be up to 50 W m^{-2} . This difference is a well-known flaw of the eddy-correlation method (Wilson et al., 2002; Foken et al., 2006). The energy balance was corrected by increasing H and λE while keeping the Bowen ratio constant. In the Fig. 4a,b the correlation is given between SEBAL and ground based corrected R_n and λE , respectively. For Matra SEBAL overestimates R_n by 4.8% and for Bugac by 8.4%, which is relatively good considering the difference in spatial scales between the observation methods. The difference between SEBAL and ground based λE is larger:

Title Page

Abstract

Introduction

Conclusions

References

Tables

Figures

◀

▶

◀

▶

Back

Close

Full Screen / Esc

Printer-friendly Version

Interactive Discussion



3% for Matra and 23.6% for Bugac. The accuracy of SEBAL evaporation estimates at a daily basis is estimated to be 10 to 15% at a spatial resolution of 0.25° (Bastiaanssen et al., 2005). On a seasonal bases the accuracy is 3–5%.

3.3.3 SEBAL evaporation in the Transdanubian region

5 In Fig. 5 the SEBAL seasonally averaged evaporative fraction $\lambda E/R_n$ is given. Data are downscaled to the model spatial resolution of 0.25° . The considered growing season covers 30 weeks and starts at week 13 (26 March 2005). The spatial pattern of $\lambda E/R_n$ is similar to the spatial pattern of precipitation shown in Fig. 3b, which suggests that $\lambda E/R_n$ is to a large extent controlled by precipitation. Figure 6 shows the relationship between annual P (mm) and seasonal E (mm) for each grid cell. For low P ($450 < P < 750$ mm), E monotonically increases with P , suggesting moisture-limited evaporation. For larger P (> 750 mm) evaporation ceases to increase, pointing to radiation-controlled evaporation. The grid cells situated above the 45° -line $E=P$ need additional recharge to sustain the evaporation rates ($P-E < 0$). This phenomenon can also be observed in Fig. 7, which shows a map of the water balance deficit (potential recharge). The red grid cells ($P-E < 0$) are situated along the river Danube, which is known to contain irrigated cropland (see Fig. 2), and could be influenced by shallow groundwater that facilitates capillary rise of water inside the soil column. These areas coincide with low precipitation areas. The blue areas, where $P-E > 200$ mm, are mainly characterized by mountainous terrain related to lateral (sub-)surface flow as well as lower soil thickness (and therefore reduced water availability and lower E).

4 HTESSEL model setup and input data

4.1 Atmospheric forcing

25 The test domain has been divided into 170 grid cells at a resolution of 0.25° . For this domain, simulations covering the entire year 2005 have been executed. HTESSEL

Title Page

Abstract

Introduction

Conclusions

References

Tables

Figures

◀

▶

◀

▶

Back

Close

Full Screen / Esc

Printer-friendly Version

Interactive Discussion



was forced using 3-hourly fields of precipitation P , radiation R_s^\downarrow and R_l^\downarrow , temperature T_{a2m} , humidity q and wind speed at 10 m height u . These fields were derived from a simulation with the *Regional Atmospheric Climate Model* (RACMO2.1; Van Meijgaard et al., 2008) driven by ECMWF operational analysis. This set-up was preferred above interpolation of ERA-40 data, to avoid imbalances in the atmospheric driving fields originating from the data assimilation applied in ERA-40 (Uppala et al., 2005). With this set-up the right synoptic variability has been retained as well as atmospheric forcing variables that were in mutual agreement. The operational land surface scheme used in RACMO2.1 was TESSEL (Van den Hurk et al., 2000). The projected average T_{a2m} over 2005 was 9.5°C and the average summer T_{a2m} was 19.8°C.

RACMO shows systematic biases as compared to observed precipitation and as compared to the radiative fluxes used to drive SEBAL. Correction procedures were applied prior to running HTESSEL using a similar approach as Sellers et al. (1996).

The weekly averaged R_n obtained through SEBAL as well as the in situ observations at Matra and Bugac was significantly higher than the values calculated by RACMO. In Fig. 8 the weekly averaged daily R_n is shown for the entire test domain. We corrected R_s^\downarrow obtained from RACMO for each model cell and 3-hourly timestep, using weekly R_n data of both SEBAL and weekly downward fluxes from RACMO:

$$R_{s\text{corr}}^\downarrow = \xi_w \cdot R_s^\downarrow \quad (6)$$

where

$$\xi_w = \frac{\langle R_{n,\text{SEBAL}} \rangle_w}{(1 - \alpha) \langle R_s^\downarrow \rangle_w + \langle R_{l,n} \rangle_w} \quad (7)$$

and $\langle R_s^\downarrow \rangle_w$ represents the weekly cell area averaged R_s^\downarrow , $\langle R_{n,\text{SEBAL}} \rangle_w$ the SEBAL weekly averaged R_n and $\langle R_{l,n} \rangle_w$ the weekly net long wave radiation from the combination of RACMO downward and HTESSEL upward obtained with a preliminary run.

Title Page

Abstract

Introduction

Conclusions

References

Tables

Figures

◀

▶

◀

▶

Back

Close

Full Screen / Esc

Printer-friendly Version

Interactive Discussion



Since, R_i^\uparrow is no SEBAL product but has been calculated by HTESSSEL, it is sensitive to R_s^\downarrow . On average $R_{s\text{corr}}^\downarrow$ is greater than R_s^\downarrow . In the preliminary calculations with HTESSSEL, the increased R_s^\downarrow resulted in an increased R_i^\uparrow and a weekly R_n that is lower than the intended $\langle R_{n,\text{SEBAL}} \rangle_w$. The maximum difference is 10%.

To improve the precipitation model input we used the TRMM product (see Sect. 3.2). The monthly TRMM precipitation was disaggregated using 3-hourly RACMO data to obtain a precipitation data series with sub-daily variation and a corrected mean. The 3-hourly precipitation, P_{corr} is:

$$P_{\text{corr}} = \chi_m \cdot P, \quad (8)$$

where $\chi_m = \frac{\langle P \rangle_{m,\text{TRMM}}}{\langle P \rangle_m}$ with $\langle P \rangle_m$ being the monthly averaged RACMO precipitation (i.e. rainfall and snowfall) and $\langle P \rangle_{m,\text{TRMM}}$ the monthly corrected TRMM precipitation at the nearest data point. On a yearly basis, the scaling factor χ_m ranged between 0.7 and 1.2.

4.2 Soil and vegetation data input of HTESSSEL

Soil hydrologic parameters were taken from the FAO soil map and database at a spatial resolution of 5' (FAO, 1995). Soil textural information of the FAO soil types has been translated to six texture classes: coarse, medium, medium-fine, fine, very fine and organic. For each of the soil texture classes the hydraulic conductivity k and the Van Genuchten coefficients α , n and m were specified (see also Van den Hurk and Viterbo, 2003). The dominant soil type was used for each grid cell. Vegetation parameters were provided by the ECOCLIMAP vegetation map (Masson et al., 2003) at a resolution of 5' and translated to high and low vegetation tiles.

Title Page

Abstract

Introduction

Conclusions

References

Tables

Figures

◀

▶

◀

▶

Back

Close

Full Screen / Esc

Printer-friendly Version

Interactive Discussion



4.3 Initial conditions of HTESSEL soil state variables

Initial water in the soil system serves as a water reservoir that is available for evaporation in times of low precipitation. A proper estimation of initial soil water and snow in the model is therefore important. HTESSEL has been run for two sets of initial conditions. These sets contain soil moisture, intercepted water, snow water mass, snow temperature, snow density and soil temperature. Set 1 consists of initial conditions from the hindcast run of RACMO driven by ECMWF operational analysis. Set 2 uses an equilibrium initial state, obtained by cycling the model through the 2005 forcing until equilibrium was reached, i.e. using the convergence criterion of less than 1.25% difference in total soil water volume. In Table 1 mean, maximum and minimum of the initial total soil water storage (mm) and the water equivalent snow thickness (mm) in the grid cells are given for Set 1 and 2. Soil water storage differs greatly between the two sets, implying a large difference in the total annual amount of water that is available for evaporation. Set 2 has considerable higher initial soil water variability and a thicker overall snow pack than Set 1. The relatively large snow layer for Set 2 is caused by the heavy snowfall at the end of 2005.

5 Results of HTESSEL calculations

The HTESSEL model skills to reproduce surface evaporation were evaluated by comparing the HTESSEL evaporative fraction $\lambda E/R_n$ with SEBAL derived $\lambda E/R_n$ for initial condition Sets 1 and 2.

In Table 2 the mean, variance and the 10th and 90th percentile of the seasonally averaged $\lambda E/R_n$ are given for SEBAL and HTESSEL Sets 1 and 2. The HTESSEL mean and 90th percentile values of $\lambda E/R_n$ correspond very well to SEBAL. The 10th percentile of HTESSEL is lower than SEBAL, which indicates a small offset towards lower $\lambda E/R_n$. The RMSE's of the model simulations are approximately 9% of the mean SEBAL $\lambda E/R_n$. This is larger than the accuracy of SEBAL, which is on a seasonal

Title Page

Abstract

Introduction

Conclusions

References

Tables

Figures



Back

Close

Full Screen / Esc

Printer-friendly Version

Interactive Discussion



basis approximately 5%.

In Fig. 9a,b the difference between SEBAL and HTESEL seasonally averaged $\lambda E/R_n$ is given as percentage of SEBAL $\lambda E/R_n$ for Set 1 and 2, respectively. The maximum prediction error is 30%. The figures reveal that initial conditions may have a large impact on the spatial distribution of calculated $\lambda E/R_n$.

To eliminate explicit spatial information, $\lambda E/R_n$ values of SEBAL and HTESEL were ranked from low to high and subsequently plotted in Fig. 10. The figure shows that model $\lambda E/R_n$ is slightly lower than SEBAL $\lambda E/R_n$ for Set 1 as well as Set 2. This is most prominent for low $\lambda E/R_n$.

In Fig. 11 calculated seasonal evaporation is plotted against yearly precipitation for SEBAL and the two model calculations. Similar to SEBAL $\lambda E/R_n$, the calculated $\lambda E/R_n$ is precipitation dominated, especially for initial condition Set 2. The figure further reveals that HTESELs skill to reproduce evaporation in areas with negative potential recharge appear to be poor for both initial condition sets.

6 Design and evaluation of modifications to HTESEL

To provide a rational approach to parameterization changes, Metselaar et al. (2006) analyzed the sensitivity of calculated turbulent surface fluxes to 15 different soil process parameterizations for two climates: Continental and Atlantic. The detailed and flexible soil-water-atmosphere model SWAP that is generally used for agrohydrological studies (Kroes et al., 2008), has been employed for this analysis. The analysis indicates that especially the treatment of the lower boundary condition (free drainage, irrigation, capillary rise from groundwater) and rooting depth, but also the depth of the soil column, may have a significant effect on the partitioning of radiant energy over latent, sensible and soil heat fluxes. Additionally, Metselaar et al. (2006) showed that transpiration timing strongly responds to a change of the evaporation reduction function, i.e. from a function of volumetric soil moisture to a function of soil water pressure head. Besides, Metselaar et al. (2006) indicated that a finer mesh of the soil column

Title Page

Abstract

Introduction

Conclusions

References

Tables

Figures

◀

▶

◀

▶

Back

Close

Full Screen / Esc

Printer-friendly Version

Interactive Discussion



yields improved convergence.

Given the results of the sensitivity analysis of Metselaar et al. (2006), we incorporated and evaluated a number of modifications to HTESSSEL that are discussed below.

6.1 The effect of water stress on the canopy resistance

5 We changed the function f_2 in Eq. (3) to a (more physically based) water pressure dependent expression as:

$$f_2^{-1} = \frac{\psi(\bar{\theta}) - \psi_{wp}}{\psi_{fc} - \psi_{wp}}, \quad (9)$$

where ψ (bar) is the soil matric pressure, defined as the air pressure minus the water pressure. The matric pressure of the permanent wilting point (ψ_{wp}) and the field capacity (ψ_{fc}) is -15 bar and -0.1 bar, respectively. For $\psi < \psi_{fc}$, f_2 decreases from 1 at field capacity to 0 at wilting point. In Fig. 12, the functions f_2 as defined by Eq. (3) and Eq. (9), respectively, have been depicted as a function of ψ . Especially in the frequently occurring ψ range between -10 and -0.2 bar the difference in reduction is large.

6.2 Soil depth classes

15 To replacing the fixed soil column depth of 2.89 m, spatially variable soil depths were constructed based on the Digital Soil Map of the World and Derived Soil Properties CD-ROM (Version 3.5, FAO, 1995). Given the soil type at the FAO soil map and the soil name, phase and drainage class, taxotransfer rules were used to determine the soil depth classes at the spatial resolution of the FAO map ($5'$). These rules have been developed by Van Dam et al. (1994) in the framework of a European Crop Growth
20 Monitoring System. The rationale behind these rules is that the soil depth of interest is on the one hand physically limited by rocky material below the soil column and on the other hand determined by the maximum rooting depth, which might be reduced due to rocks and/or rocky material in the soil. For example, the soil depth of lithosols is

Title Page

Abstract

Introduction

Conclusions

References

Tables

Figures

◀

▶

◀

▶

Back

Close

Full Screen / Esc

Printer-friendly Version

Interactive Discussion



Title Page

Abstract

Introduction

Conclusions

References

Tables

Figures

◀

▶

◀

▶

Back

Close

Full Screen / Esc

Printer-friendly Version

Interactive Discussion



only 10 cm, and the soil depth of histosols and arenosols is 60 cm. We distinguished between five soil depth classes: soil depths of 10, 60, 80, 100 cm and >100 cm (i.e. 2.89 m). A map of soil depths in the test region is given in Fig. 13a. 30% of the test region has a soil depth that is shallower than 2.89 m. For this part of the region, the original model input soil depth has to be changed to more physically realistic depths.

6.3 Shallow groundwater

As no upward flow from groundwater is possible in the current HTESSEL model, this effect is represented by introducing extra storage for soils with shallow groundwater. For this the van Genuchten retention parameter α was changed such that the effective soil moisture at field capacity increased by 10%, i.e. $\frac{\theta_{fc}^* - \theta_r}{\theta_{sat} - \theta_r} = 1.1 \frac{\theta_{fc} - \theta_r}{\theta_{sat} - \theta_r}$ (where * refers to the new updated situation) while retaining free drainage as the imposed bottom boundary condition. In fact, the effect of this modification is a decreased relative conductivity at the same soil moisture content. The rephrased α is solved from

$$\theta_{fc} = \theta_r + \frac{\theta_{sat} - \theta_r}{(1 + (\alpha h_{fc})^n)^{1-1/n}} \quad (10)$$

where θ_{sat} , θ_r are the soil moisture at full saturation and residual saturation, respectively, n and α are soil specific parameters and $h_{fc} = \psi / (\rho_w g)$. Then:

$$\alpha^* = h_{fc}^{-1} [\chi(1 + (\alpha h_{fc})^n) - 1]^{1/n}, \quad (11)$$

where $\chi = (1.1)^{-1/(1-1/n)}$. To obtain a global map of soils influenced by shallow groundwater, the method proposed by Van Dam et al. (1994) was applied to FAO soil type data, i.e. Gleysoils, Phaeozems, Fluvisols, Histosols, Gleyic Podsoils were labeled as being groundwater affected. Figure 13b shows the affected grid cells in the test region.

6.4 Evaluation of the HTESSSEL modifications

Four cases have been evaluated, and compared to the reference HTESSSEL. In Case 1 f_2 was revised. In Case 2 a variable soil depth was applied. Case 3 considers the effect of shallow groundwater. Case 4 combines Cases 1, 2 and 3. Additionally, we doubled the number of soil layer from 4 to 8 for all Cases. We used two sets of initial conditions (see Table 1). The evaluated Cases are listed in Table 3.

Statistical properties of the calculated evaporative fractions are given in Table 4 for each case. Also the correlation coefficients between SEBAL and HTESSSEL evaporation are given. In Fig. 14a,b the ranked $\lambda E/R_n$ are given for SEBAL and the cases considered for initial condition Sets 1 and 2, respectively.

For Case 1 the mean $\lambda E/R_n$ and variance increase with respect to the reference HTESSSEL for Set 1 as well as Set 2. The increase of $\lambda E/R_n$, is consistent with the new f_2 function that shows less root water uptake reduction for similar ψ and thus increased evaporation. However, the $\lambda E/R_n$ is too high compared to SEBAL $\lambda E/R_n$ and the RMSE is therefore larger than for the reference HTESSSEL.

For Case 2 the mean evaporation decreases and the 10 percentile decreases as well as compared to the reference HTESSSEL. The decreased evaporation is due to decreased moisture storage capacity for soil depths less than 2.89 m, i.e. in shallow soils the soil water is depleted more easily. Although additional spatial soil information is added, it only results in slightly increased variability of the calculated evaporation. The correlation coefficient between SEBAL and HTESSSEL evaporation decreased.

In Case 3 little improvement can be observed compared to the reference HTESSSEL. The statistical properties of Case 3 are similar to that of the reference runs. We may thus conclude that to increase E the chosen parameterization does not increase the available water significantly.

For Case 4, the parameterization of Case 1 and Case 3 (increase of $\lambda E/R_n$) are expected to balance the effect of Case 2 (decrease of $\lambda E/R_n$). However, the effect of the new f_2 function appears to dominate the effect of the reduced soil depth. In

Title Page

Abstract

Introduction

Conclusions

References

Tables

Figures



Back

Close

Full Screen / Esc

Printer-friendly Version

Interactive Discussion



particular this can be observed for larger $\lambda E/R_n$ (see Fig. 14a, b and also the 90th percentiles).

For all cases the correlation between the calculated evaporation and that of SEBAL was less than the reference case, except for Case 2 and initial condition Set 1, which indicates that the model skill of HTESSEL to reproduce the spatially variable evaporation has not been improved by the modifications.

7 General discussion and conclusions

The primary objective of this study is to assess the model skill of the land surface scheme HTESSEL to reproduce spatial patterns of surface evaporation in response to patterns in precipitation and land surface characteristics, with emphasis on the mean and spatial variability during dry (summer) periods. The secondary goal is to assess the effect of a number of model modifications.

We evaluated HTESSEL based evaporation on MODIS-satellite based evaporation for the Transdanubian Region in Hungary over 2005. The energy-partitioning algorithm SEBAL has been used to calculate the energy balance terms from satellite observations. The accuracy of the SEBAL latent heat flux density, λE , is approx. 3–5%, at the used spatial resolution of 0.25° on a seasonal basis. For the land surface model, off-line atmospheric forcing variables at a 3-hourly time interval were taken from a hindcast run of the regional climate model RACMO nested in ECMWF operational analysis. It was found necessary to rescale downward short-wave radiation R_s , and precipitation P , in order to match with the satellite-based observations.

The evaluation shows that, within the test region, HTESSEL predicts the seasonal energy partitioning of the incoming radiation over latent and sensible heat flux densities reasonable well, given the spatial and temporal resolution and the considered year 2005. The statistical properties of the seasonal evaporative fraction $\lambda E/R_n$ of HTESSEL and SEBAL are of the same magnitude, however, HTESSEL slightly underestimates $\lambda E/R_n$, especially for grid cells with low $\lambda E/R_n$. The RSME of HTESSEL is

Title Page

Abstract

Introduction

Conclusions

References

Tables

Figures

◀

▶

◀

▶

Back

Close

Full Screen / Esc

Printer-friendly Version

Interactive Discussion



approximately twice the accuracy of SEBAL. The prediction error of the individual grid cells is up to 30% of the SEBAL $\lambda E/R_n$. The correlation coefficient of the calculated evaporation to SEBAL evaporation is between 0.62 and 0.71, dependent on the initial conditions used.

5 These results are based on atmospheric forcing of which the accuracy is unknown. Especially precipitation P may have a large impact on the calculated evaporation E (see also Fig. 11) and a slight change in precipitation may change the calculated evaporative fractions. Longer evaluation periods are needed to confirm the observations.

The spatial distribution of the prediction error is different for two initial condition sets.

10 These sets differ in the initial conditions of soil water and snow taken from a RACMO hindcast run in Set 1 and an equilibrium state over 2005 in Set 2. The use of the two different initial condition sets, that largely reflect initial water in the terrestrial system available for evaporation, resulted in different spatial distributions of $\lambda E/R_n$. A closer look shows a great similarity between the spatial pattern of the potential recharge (Fig. 7) and the relative prediction error (accuracy) using Set 2 (Fig. 9b). This is confirmed by the calculated correlation coefficients between potential recharge and relative prediction error, which are 0.55 and 0.8 for Set 1 and 2, respectively. HTESSEL's ability to predict negative potential recharge appears to be lower than for positive potential recharge. During drier years than 2005 (which had an annual precipitation anomaly of 40 mm compared to the climatological mean of 612 mm), the prediction error may become larger.

25 The importance of representing correctly initial terrestrial water storages such as soil water and snow cover for modulating wet and dry meteorological anomalies is illustrated in Fig. 11, which shows yearly precipitation P plotted against seasonal evaporation E of each individual grid cell. E of Set 1 has a scattered relationship to P , whereas Set 2 shows a largely linear relationship. Due to the cycling over 2005, the initial state of Set 2 reflects only the signature of the atmospheric forcing over 2005, which is dominated by P in the region considered. Instead, in Set 1 the initial water stored in the soil and snow pack reflects the signal of longer-term meteorological

HTESSEL evaluation

E. L. Wipfler et al.

Title Page

Abstract

Introduction

Conclusions

References

Tables

Figures



Back

Close

Full Screen / Esc

Printer-friendly Version

Interactive Discussion



conditions. In grid cells with low precipitation over 2005, the effect on $\lambda E/R_n$ may be moderated by the relatively wet soil moisture conditions originating from a previous (winter) period. The overall effect is a more scattered relationship between P en E .

Although longer evaluation periods are needed to confirm the results, the simulations performed with HTESSSEL reveal a relatively low ability of the model to correctly predict E in areas where $P-E < 0$. Since the low precipitation areas coincide with irrigated areas, the underestimation of $\lambda E/R_n$ in grid cells with $(P-E) < 0$, might also point towards enhanced evaporation due to irrigated cropland. HTESSSEL does neither incorporate the effect of irrigation, nor the effect of shallow groundwater on the water balance. Especially, during periods with high temperatures and low humidity, additional evaporation is expected due to the availability of irrigation and groundwater. Like other Land Surface Schemes (LSS), HTESSSEL does not allow for lateral redistribution of precipitation due to surface and subsurface flow. LSSs are now being modified to include lateral flow, groundwater flow and surface water (e.g. Fan et al., 2007; Miguez-Macho et al., 2007), however these developments are still in an experimental stage. This is largely due to encountered difficulties to obtain the required hydrological data that needs global coverage and a correct resolution. By bridging the gap between hydrological and climate models and thus by incorporating lateral flow, including groundwater flow, irrigation and river routing, LSS skills may significantly improve.

Based on earlier sensitivity analysis of soil hydrologic processes (Metselaar et al., 2006) we (i) revised the parameterization of the reduction of evaporation for dry vegetation, (ii) replaced the fixed soil depth with more realistic and variable soil depths, and (iii) introduced additional water availability due to capillary rise from shallow water tables. These modifications lead to increased spatial variability of soil hydrological processes, but they did not lead to significant improvement. (i) increased the $\lambda E/R_n$ too much, especially for grid cells in the higher $\lambda E/R_n$ range, (ii) decreased on $\lambda E/R_n$ (especially in the lower range) and increased the RMSE. The unrealistically large soil thickness in HTESSSEL seems to compensate for the strong reduction of root water uptake under dry conditions. At higher spatial resolutions the spatial variability of soil and

HTESSSEL evaluation

E. L. Wipfler et al.

Title Page

Abstract

Introduction

Conclusions

References

Tables

Figures

◀

▶

◀

▶

Back

Close

Full Screen / Esc

Printer-friendly Version

Interactive Discussion



vegetation characteristics may become more important and a more physically based description of soil moisture movement may be warranted. (iii) did not lead to significant changes in $\lambda E/R_n$. A more rigorous parameterization for the groundwater dynamics may be needed to improve the models ability of predicting evaporative fractions in regions affected by shallow groundwater.

Acknowledgements. The published work was carried out within the Dutch Climate Changes Spatial Planning Program. We thank M. Vazifedoust for the translation of the FAO soil map to maps of soil depth classes and groundwater affected areas.

References

- Balsamo, G., Viterbo, P., Beljaars, A., van den Hurk, B., Hirschi, M., Betts, A. K., and Scipal, K.: A revised hydrology for the ECMWF model: Verification from field site to terrestrial water storage and impact in the Integrated Forecast System, *J. Hydrometeorol.*, 10, 623–643, 2009.
- Bastiaanssen, W. G. M., Menenti, M., Feddes, R. A., and Holtslag, A. A. M.: The Surface Energy Balance for Land (SEBAL): Part 1 formulation, *J. Hydrol.*, 212–213, 198–212, 1998.
- Bastiaanssen, W. G. M., Noordman, E. J. M., Pelgrum, H., Davids, G., Thoreson, B. P., and Allen, R. G.: SEBAL model with remotely sensed data to improve water-resources management under actual field conditions, *J. Irrig. Drain. E.-ASCE*, 131, 85–93, 2005.
- Betts, A. K., Ball, J. H., Beljaars, A. C. M., Miller, M. J., and Viterbo, P. A.: The land surface-atmosphere interaction: A review based on observational and global modeling perspectives, *J. Geophys. Res.*, 101, 7209–7225, 1996.
- De Bruin, H. A. R. and Stricker, J. N. M.: Evaporation of grass under non-restricted soil moisture conditions, *Hydrolog. Sci. J.*, 45(3), 391–406, 2000.
- Dümenil, L. and Todini, E.: A rainfall-runoff scheme for use in the Hamburg climate model. *Advances in Theoretical Hydrology, a tribute to James Dooge*, edited by: O’Kane, P., European Geophysical Society Series on Hydrological Sciences 1, Elsevier, Amsterdam, 1992.
- ECMWF: ECMWF Documentation Cycle CY28r1, part 4: Physical processes, Chapt. 7: Surface parameterization, available via <http://www.ecmwf.int/research/ifsdoc/CY31r1/index.html>, 2007.

Title Page

Abstract

Introduction

Conclusions

References

Tables

Figures



Back

Close

Full Screen / Esc

Printer-friendly Version

Interactive Discussion



Title Page

Abstract

Introduction

Conclusions

References

Tables

Figures

◀

▶

◀

▶

Back

Close

Full Screen / Esc

Printer-friendly Version

Interactive Discussion



Fan, Y., Miguez-Macho, G., Weaver, C. P., Walko, R., and Robock, A.: Incorporating water table dynamics in climate modeling: 1. Water table observations and equilibrium water table simulations, *J. Geophys. Res.*, 112, D10125, doi:10.1029/2006JD008111, 2007.

FAO: Digital soil map of the world and derived soil properties, Version 3.5, Food and Agriculture Organization of the United Nations, Rome, Italy, 1995.

Fischer, E. M., Seneviratne, S. I., Lüthi, D., and Schär, C.: Contribution of land-atmosphere coupling to recent European summer heat waves, *Geophys. Res. Lett.*, 34, L06707, doi:10.1029/2006GL029068, 2007.

Foken, T., Wimmer, F., Mauder, M., Thomas, C., and Liebenthal, C.: Some aspects of the energy balance closure problem, *Atmos. Chem. Phys.*, 6, 4395–4402, 2006, <http://www.atmos-chem-phys.net/6/4395/2006/>.

Hagemann, S., Machenhauer, B., Jones, R., Christensen, O. B., Déqué, M., Jacob, D., and Vidale, P. L.: Evaluation of water and energy budgets in regional climate models applied over Europe, *Clim. Dynam.*, 23, 547–567, 2004.

Hirschi, M., Seneviratne, S., and Schär, C.: Seasonal variations in terrestrial water storage for major mid-latitude river basins, *J. Hydrometeorol.*, 7, 39–60, 2006.

Jarvis, P. G.: The interpretation of the variations in leaf water potential and stomatal conductance found in canopies in the field, *Philos. T. Roy. Soc. B*, 273, 593–610, 1976.

Kroes, J. G., van Dam, J. C., Groenendijk, P., Hendriks, R. F. A., and Jacobs, C. M. J.: SWAP version 3.2, Theory description and user manual, Alterra report 1649, Alterra, Wageningen, 2008.

Lenderink, G., van den Hurk, B., van Meijgaard, E., van Ulden, A., and Cuijpers, H.: Simulation of present-day climate in RACMO2: First results and model developments, *KNMI tech. report 252*, 24 p., 2003.

Masson, V., Champeaux, J.-L., Chauvin, F., Meriquet, C., and Lacaze, R.: A Global database of land surface parameters at 1-km resolution in meteorological and climate models, *J. Climate*, 16(9), 1261–1282, 2003.

Metselaar, K., van Dam, J. C., and Feddes, R. A.: Screening and understanding the importance of soil hydrology related factors in a SVAT scheme, Report in the framework of the Climate Changes Spatial Planning Program, project CS3: Representation of soil moisture and root water uptake in climate models, online available at: <http://programmabureauklimaat.nl>, 2006.

Miguez-Macho, G., Fan, Y., Weaver, C. P., Walko, R., and Robock, A.: Incorporating water

HTESSEL evaluation

E. L. Wipfler et al.

Title Page

Abstract

Introduction

Conclusions

References

Tables

Figures

◀

▶

◀

▶

Back

Close

Full Screen / Esc

Printer-friendly Version

Interactive Discussion



- table dynamics in climate modeling: 2. Formulation, validation, and soil moisture simulation, *J. Geophys. Res.*, 112, D13108, doi:10.1029/2006JD008112, 2007.
- Sellers, P. J., Meeson, B. W., Closs, J., Collatz, J., Corprew, F., Dazlich, D., Hall, F. G., Kerr, Y., Koster, R., Los, S., Mitchell, K., McManus, J., Myers, D., Sun, K. J., Try, P.: The ISLSCP initiative I global datasets: Surface boundary conditions and atmospheric forcings for land-atmosphere studies, *B. Am. Meteorol. Soc.*, 77, 1987–2005, 1996.
- Seneviratne, S. I., Viterbo, P., Lüthi, D., and Schär, C.: Inferring changes in terrestrial water storage using ERA-40 reanalysis data: The Mississippi River basin, *J. Climate*, 17, 2039–2057, 2004.
- Siebert, S., Döll, P., Feick, S., Hoogeveen, J., and Frenken, K.: Global Map of Irrigation Areas version 4.0.1., Johann Wolfgang Goethe University, Frankfurt am Main, Germany/Food and Agriculture Organization of the United Nations, Rome, Italy, 2007.
- Szalai, S., Bihari, Z., Lakatos, M., Szentimrey, T.: Some characteristics of the climate of Hungary since 1901, Hungarian Meteorological Service Report, Budapest, Hungary, 2005.
- Tuba, Z., Nagy, Z., and Csintalan, Z.: CarboeuropelP Ecosystem Component Database, available via: <http://gaia.agraria.unitus.it/database>, 2005.
- Uppala, S. M., Kållberg, P. W., Simmons, A. J., Andrae, U., da Costa Bechtold, V., Fiorino, M., Gibson, J. K., Haseler, J., Hernandez, A., Kelly, G. A., Li, X., Onogi, K., Saari-
 20 jaars, A. C. M., van de Berg, L., Bidlot, J., Bormann, N., Caires, S., Chevallier, F., Dethof, A., Dragosavac, M., Fisher, M., Fuentes, M., Hagemann, S., Hólm, E., Hoskins, B. J., Isak-
 25 sen, L., Janssen, P. A. E. M., Jenne, R., McNally, A. P., Mahfouf, J.-F., Morcrette, J.-J., Rayner, N. A., Saunders, R. W., Simon, P., Sterl, A., Trenberth, K. E., Untch, A., Vasilje-
 vic, D., Viterbo, P., and Woollen, J.: The ERA-40 re-analysis, *Q. J. Roy. Meteor. Soc.*, 131, 2961–3012, doi:10.1256/qj.04.176, 2005.
- Van Dam, O., van der Drift, J. W. M., and van Diepen, C. A.: Estimation of the Available Soil Moisture Capacity for the soil units of the EC soil map, DLO Winand Staring Centre, Wageningen, the Netherlands, Technical Document 20, p. 88, 1994.
- Van den Hurk, B. and Viterbo, P.: The Torne-Kalix PILPS 2(e) experiment as a test bed for modifications to the ECMWF land surface scheme, *Global Planet. Change*, 38, 165–173, 2003.
- Van den Hurk, B. J. J. M., Viterbo, P., Beljaars, A. C. M., and Betts, A. K.: Offline validation of the ERA40 surface scheme; ECMWF TechMemo 295, see <http://www.ecmwf.int/>

- publications/library/ecpublications/_pdf/tm/001-300/tm295.pdf, 2000.
- Van den Hurk, B. J. J. M., Graham, P., and Viterbo, P.: Comparison of land surface hydrology in regional climate simulations of the Baltic Sea catchment, *J. Hydrol.*, 255, 169–193, 2002.
- Van Genuchten, M.: A closed form equation for predicting the hydraulic conductivity of unsaturated soils, *Soil Sci. Soc. Am. J.*, 44, 892–898, 1980.
- 5 Van Meijgaard, E., van Ulfst, L. H., van de Berg, W. J., Bosveld, F. C., van den Hurk, B. J. J. M., Lenderink, G., Siebesma, A. P.: The KNMI regional atmospheric climate model RACMO, version 2.1, KNMI Technical Report 302, 43 pp., 2008
- Viterbo, P. and Beljaars, A. C. M.: An improved land surface parameterization scheme in the ECMWF model and its validation, *J. Climate*, 8, 2716–2748, 1995.
- 10 Viterbo, P., Beljaars, A., Mahfouf, J.-F., and Teixeira, J.: The representation of soil moisture freezing and its impact on the stable boundary layer, *Q. J. Roy. Meteor. Soc.*, 125, 2401–2426, 1999.
- Voogt, M. P.: Meteolook-a physically based regional distribution model for measured meteorological variables, M.Sc. thesis Delft University of Technology, Delft, The Netherlands, 2006.
- 15 Wilson, K. B., Goldstein, A. H., Falge, E., Aubinet, M., Baldocchi, D., Berbigier, P., Bernhofer, C., Ceulemans, R., Dolman, H., Field, C., Grelle, A., Law, B., Meyers, T., Moncrieff, J., Monson, R., Oechel, W., Tenhunen, J., Valentini, R., and Verma, S.: Energy balance closure at FLUXNET sites, *Agr. Forest Meteorol.*, 113, 223–243, 2002.
- 20 Zeng, X., Dai, Y.-J., Dickinson, R. E., and Shaikh, M.: The role of root distribution for climate simulation over land, *Geophys. Res. Lett.*, 25(24), 4533–4536, 1998.

HTESSEL evaluation

E. L. Wipfler et al.

Title Page

Abstract

Introduction

Conclusions

References

Tables

Figures



Back

Close

Full Screen / Esc

Printer-friendly Version

Interactive Discussion



Table 1. Mean, maximum and minimum model grid values of initial soil water storage and initial water equivalent snow (mm). Set 1 is the initial condition set that originates from the RACMO hindcast run, Set 2 is the equilibrium initial condition state.

	Soil water storage (mm)		Water equivalent snow (mm)	
	Set 1	Set 2	Set 1	Set 2
Mean	782	732	0.2	20
Minimum	625	241	0	1
Maximum	967	1150	2	51

Title Page

Abstract

Introduction

Conclusions

References

Tables

Figures

◀

▶

◀

▶

Back

Close

Full Screen / Esc

Printer-friendly Version

Interactive Discussion



HTESSEL evaluation

E. L. Wipfler et al.

Table 2. Mean, 10th and 90th percentile of $\lambda E/R_n$ from SEBAL and HTESSEL for the initial condition Set 1 and Set 2. The RMSE of the HTESSEL model predictions is given in the last row.

	SEBAL	HTESSEL, Set 1	HTESSEL, Set 2
Mean $\lambda E/R_n$	0.64	0.62	0.62
10th percentile $\lambda E/R_n$	0.56	0.53	0.54
90th percentile $\lambda E/R_n$	0.71	0.70	0.71
RMSE $\lambda E/R_n$	–	0.06	0.055

Title Page

Abstract

Introduction

Conclusions

References

Tables

Figures

◀

▶

◀

▶

Back

Close

Full Screen / Esc

Printer-friendly Version

Interactive Discussion



HTESSEL evaluation

E. L. Wipfler et al.

Table 3. Evaluated combinations of the proposed modifications to HTESSEL. Four configurations (cases) were considered. The differences with respect to the reference HTESSEL is indicated in bold.

Case	Reference	1	2	3	4
f_2 dependency	θ	ψ	θ	θ	ψ
soil depth	2.89 m	2.89 m	variable	2.89 m	variable
groundwater effect	No	no	No	Yes	yes
Number of compartments	4	8	8	8	8

Title Page

Abstract

Introduction

Conclusions

References

Tables

Figures

◀

▶

◀

▶

Back

Close

Full Screen / Esc

Printer-friendly Version

Interactive Discussion



Table 4. Summary statistics of the calculated evaporative fractions evaluated cases.

Case	reference		1		2		3		4	
	1	2	1	2	1	2	1	2	1	2
Set										
Mean $\lambda E/R_n$	0.62	0.62	0.7	0.69	0.60	0.60	0.62	0.63	0.67	0.66
10%-ile $\lambda E/R_n$	0.53	0.54	0.58	0.58	0.51	0.51	0.53	0.54	0.55	0.54
90%-ile $\lambda E/R_n$	0.70	0.71	0.79	0.80	0.70	0.71	0.71	0.71	0.79	0.78
RMSE $\lambda E/R_n$	0.06	0.06	0.09	0.08	0.07	0.07	0.06	0.05	0.08	0.08
Corr. Coeff of E	0.62	0.71	0.52	0.65	0.66	0.70	0.60	0.70	0.54	0.64

Title Page

Abstract

Introduction

Conclusions

References

Tables

Figures



Back

Close

Full Screen / Esc

Printer-friendly Version

Interactive Discussion



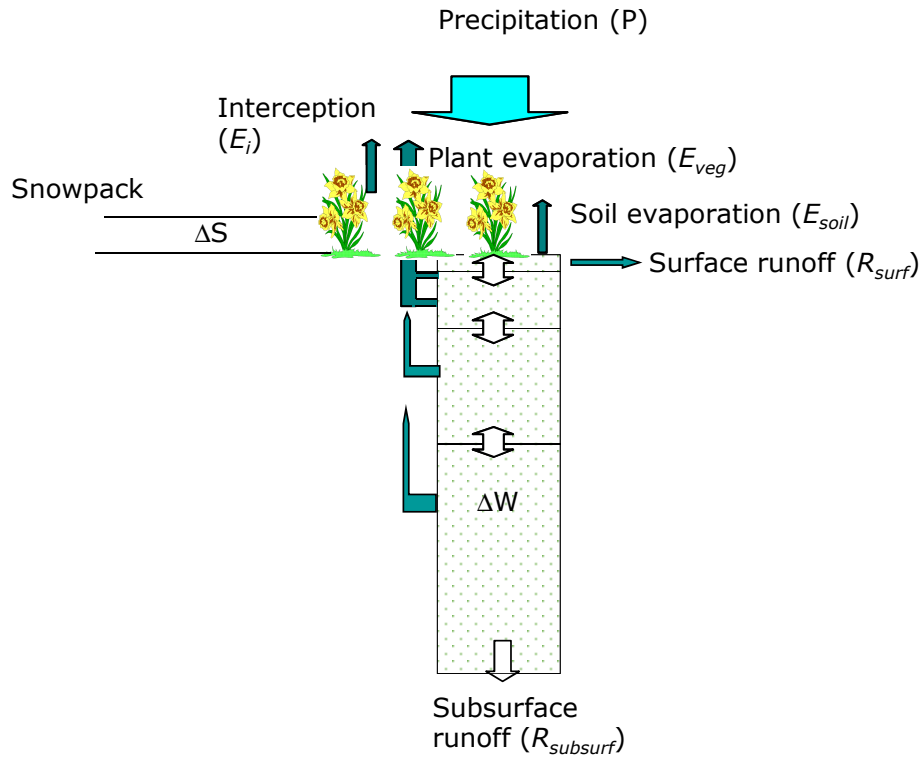


Fig. 1. Water balance of the land surface scheme HTESSEL.

Title Page

Abstract

Introduction

Conclusions

References

Tables

Figures

◀

▶

◀

▶

Back

Close

Full Screen / Esc

Printer-friendly Version

Interactive Discussion



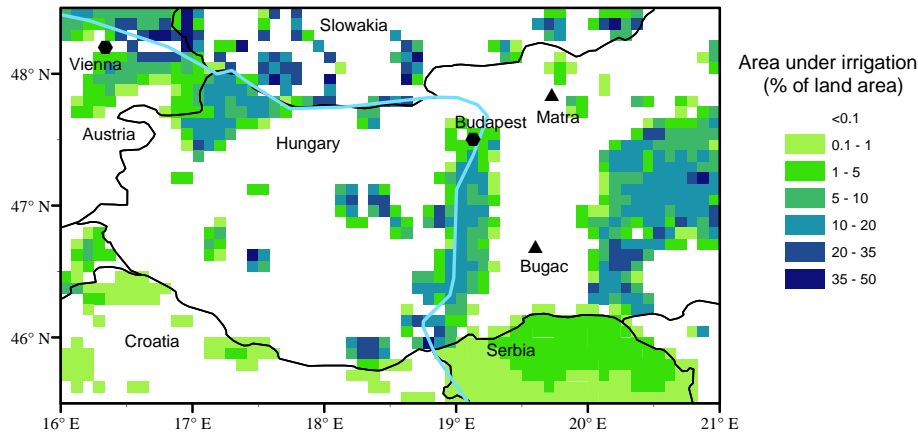


Fig. 2. Transdanubian test region and percentage of irrigated area obtained from the global map of irrigation areas provided by the FAO’s global information system on water and agriculture at a resolution of 5’ (Siebert et al., 2007). The black lines represent country boundaries. The light blue line indicates the river Danube. The locations of the meteorological towers Matra and Bugac are indicated with black triangles.

Title Page	
Abstract	Introduction
Conclusions	References
Tables	Figures
◀	▶
◀	▶
Back	Close
Full Screen / Esc	
Printer-friendly Version	
Interactive Discussion	



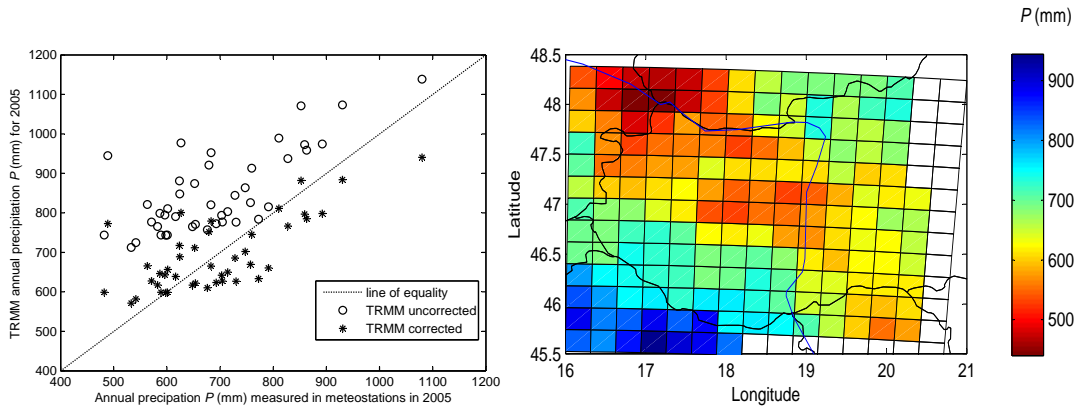


Fig. 3. Annual precipitation P (mm) over 2005 in the test area **(a)** measured at meteorostations and the corresponding corrected and uncorrected TRMM observations and **(b)** corrected TRMM observations being projected at a spatial resolution of 0.25° .

Navigation menu:

- Title Page
- Abstract
- Introduction
- Conclusions
- References
- Tables
- Figures
- Navigation arrows: left, right, back, forward
- Back
- Close
- Full Screen / Esc
- Printer-friendly Version
- Interactive Discussion



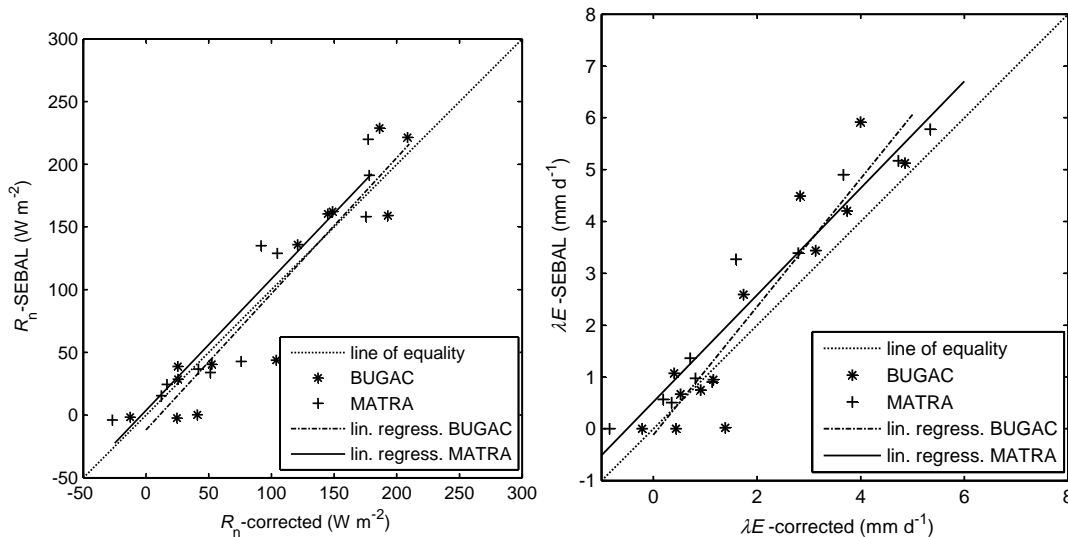


Fig. 4. (a) Correlation between groundbased R_n and R_n -SEBAL. (b) Correlation between groundbased corrected λE (mm d^{-1}) and λE -SEBAL. The groundbased energy fluxes have been obtained from the meteorological towers Matra and Bugac, of which the energy balances have been closed proportional to the Bowen ratio.

Title Page

Abstract

Introduction

Conclusions

References

Tables

Figures

◀

▶

◀

▶

Back

Close

Full Screen / Esc

Printer-friendly Version

Interactive Discussion



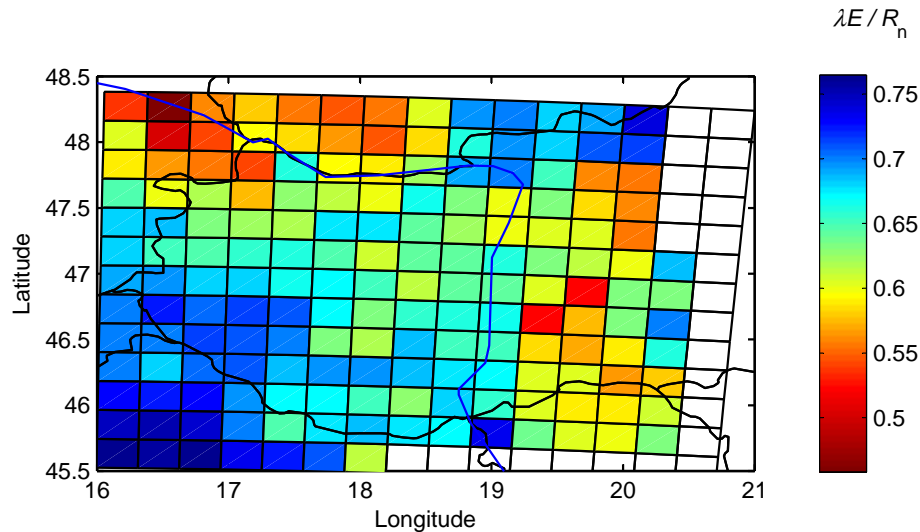


Fig. 5. Map of seasonally averaged daily $\lambda E / R_n$ for the Transdanubian test region in 2005. $\lambda E / R_n$ has been derived from satellite images using SEBAL. The spatial resolution is 0.25° .

Title Page

Abstract

Introduction

Conclusions

References

Tables

Figures

◀

▶

◀

▶

Back

Close

Full Screen / Esc

Printer-friendly Version

Interactive Discussion



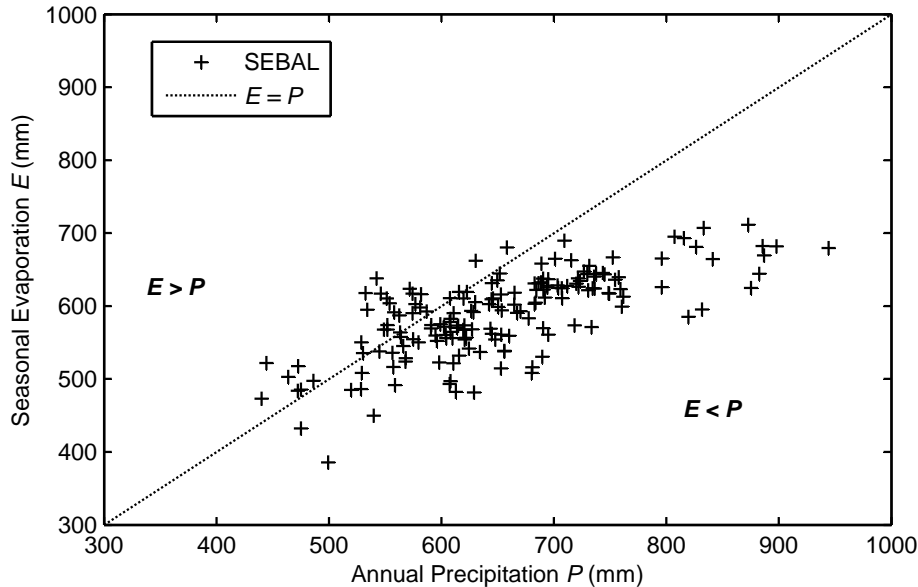


Fig. 6. Seasonal SEBAL derived evaporation E (mm) over a 30 week period in 2005 starting at week 13 and ending at week 43 and annual TRMM precipitation P (mm) over 2005 for each grid cell in the test region. Each point represents a grid cell. The line $E = P$ (dotted) is given for reference.

Title Page

Abstract

Introduction

Conclusions

References

Tables

Figures

◀

▶

◀

▶

Back

Close

Full Screen / Esc

Printer-friendly Version

Interactive Discussion



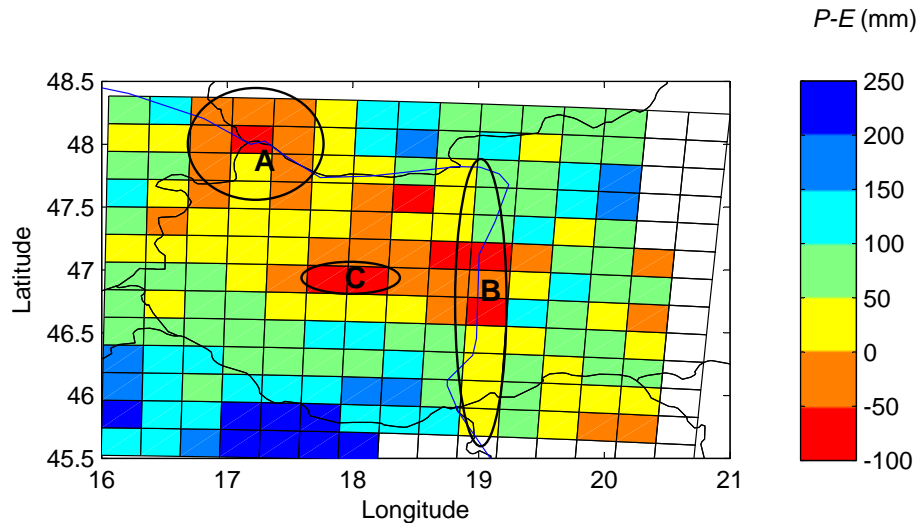


Fig. 7. Potential recharge (Annual P_{TRMM} – Seasonal E_{SEBAL}) over 2005 in the Transdanubian region. The areas A and B represent irrigated cropland area and C represents lake Balaton. The spatial resolution is 0.25° .

Title Page

Abstract

Introduction

Conclusions

References

Tables

Figures

◀

▶

◀

▶

Back

Close

Full Screen / Esc

Printer-friendly Version

Interactive Discussion



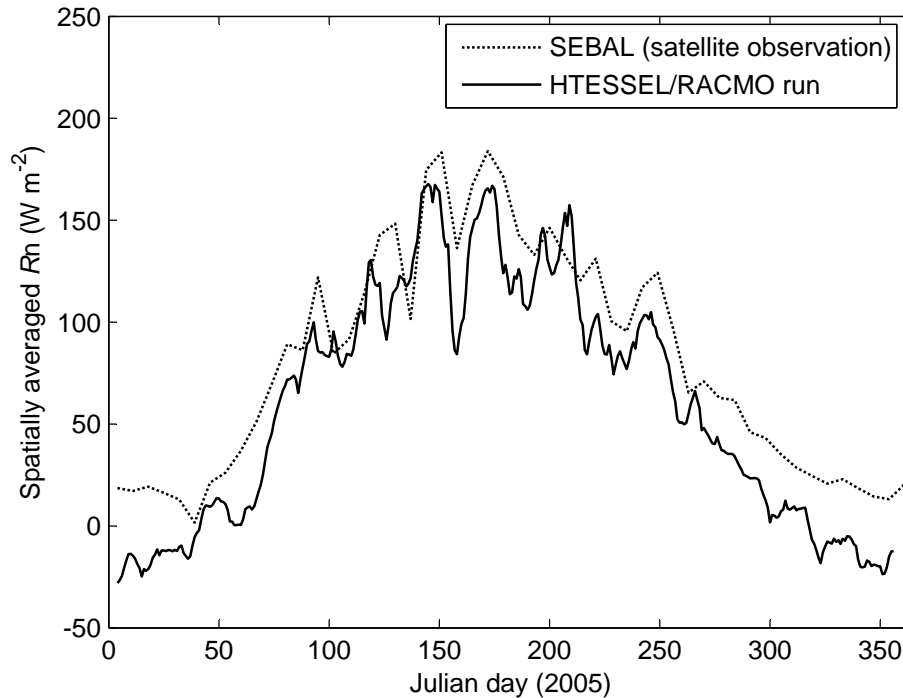


Fig. 8. Weekly averaged, daily net radiation R_n over 2005, as obtained by the SEBAL algorithm and from the HTESSEL/RACMO simulation, respectively, being averaged over the test area. The meteorological forcing and initial conditions were obtained from a one-year RACMO2-hindcast run driven by ECMWF operational analyses.

Title Page

Abstract

Introduction

Conclusions

References

Tables

Figures

◀

▶

◀

▶

Back

Close

Full Screen / Esc

Printer-friendly Version

Interactive Discussion



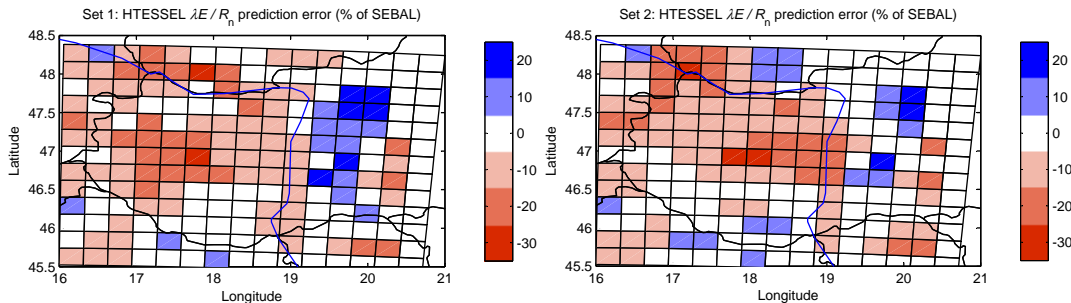


Fig. 9. Difference between SEBAL and HTESSEL seasonally averaged evaporative fraction, $\lambda E/R_n$ as percentage of SEBAL $\lambda E/R_n$ for initial condition **(a)** Set 1 and **(b)** Set 2, respectively. The blue cells refer to $\lambda E/R_n$ overprediction, the red cells to underprediction by the model.

Title Page

Abstract

Introduction

Conclusions

References

Tables

Figures

◀

▶

◀

▶

Back

Close

Full Screen / Esc

Printer-friendly Version

Interactive Discussion



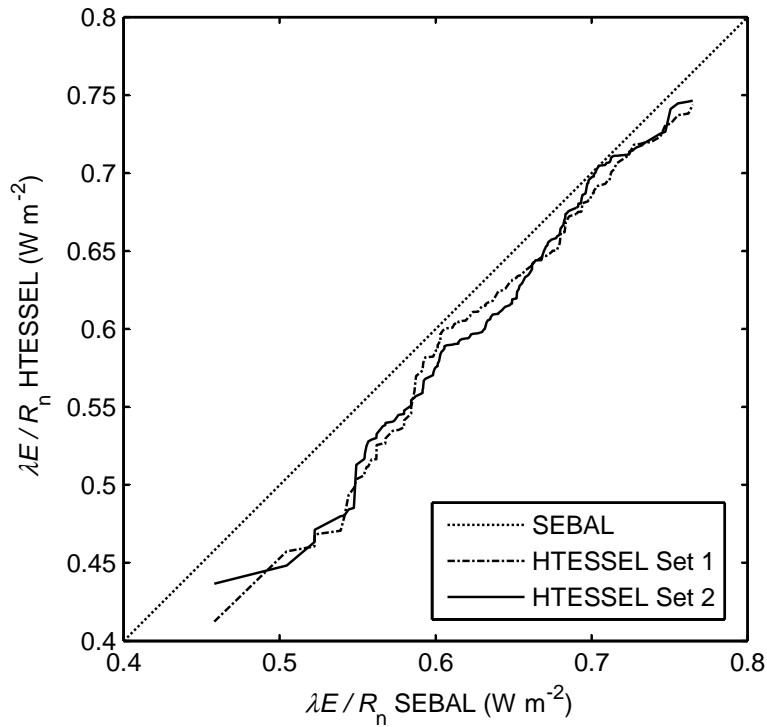


Fig. 10. HTESSSEL evaporative fraction $\lambda E/R_n$ values for each grid cell being ranked from low to high values and plotted against ranked SEBAL $\lambda E/R_n$.

Title Page

Abstract

Introduction

Conclusions

References

Tables

Figures

◀

▶

◀

▶

Back

Close

Full Screen / Esc

Printer-friendly Version

Interactive Discussion



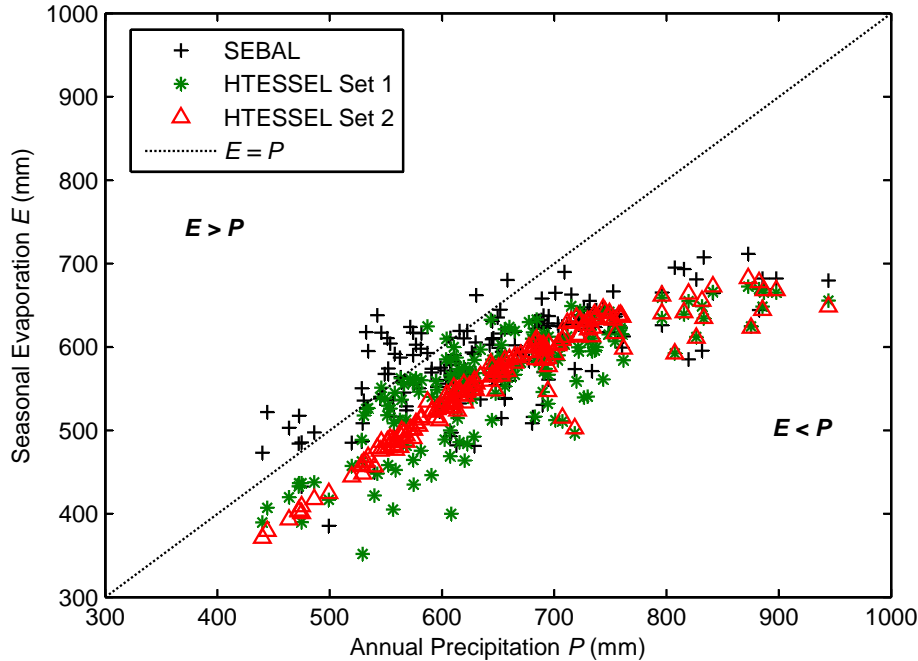


Fig. 11. Seasonal SEBAL and HTESSEL derived E (mm) over a 30 week period starting at week 13 and ending at week 43, 2005 and annual TRMM precipitation (P , mm) over 2005 for each grid cell in the test region. Each point represents one grid cell. The dotted line $E = P$ and SEBAL E are given for reference. Like Fig. 6, the figure shows a correlation between P and E , especially for Set 2. For both initial condition sets the transition between precipitation dominated E and radiation dominated E is clearly visible.

Title Page

Abstract

Introduction

Conclusions

References

Tables

Figures

◀

▶

◀

▶

Back

Close

Full Screen / Esc

Printer-friendly Version

Interactive Discussion



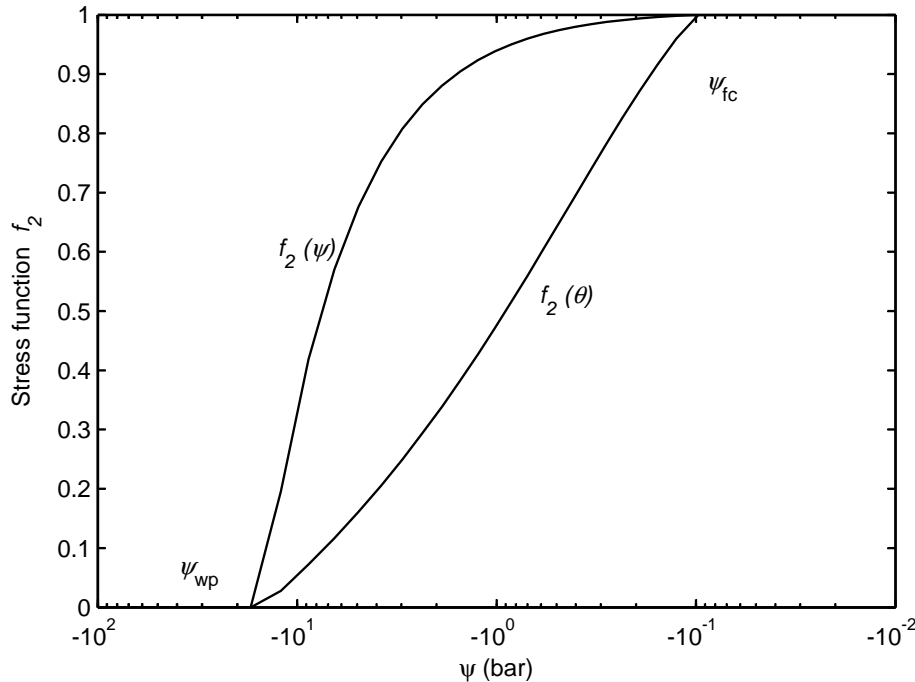


Fig. 12. The functions $f_2(\theta)$ and $f_2(\psi)$ as related to soil matric pressure. The hydraulic properties of the soil are: $k=0.26e^{-6}$ ($m s^{-1}$), $n=1.25$, $\alpha=0.83 m^{-1}$, $\theta_{max}=0.43$ and $\theta_r=0.01$. The functions $f_2(\theta)$ and $f_2(\psi)$ have been calculated according to Eqs. (3) and (9), respectively.

Title Page

Abstract

Introduction

Conclusions

References

Tables

Figures

◀

▶

◀

▶

Back

Close

Full Screen / Esc

Printer-friendly Version

Interactive Discussion



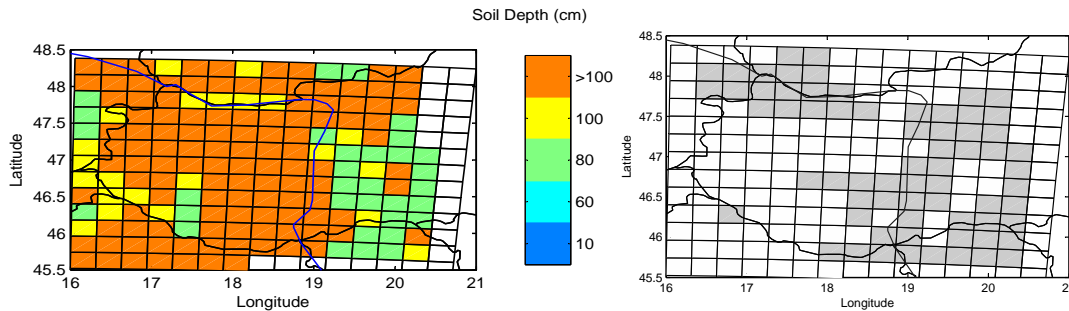


Fig. 13. (a) Soil depth classes and (b) groundwater affected soils (dark cells) occurring in the test region, as based on FAO soil classification and expected rooting depth and aggregated to the spatial resolution of 0.25° .

Title Page

Abstract

Introduction

Conclusions

References

Tables

Figures



Back

Close

Full Screen / Esc

Printer-friendly Version

Interactive Discussion



HTESSEL evaluation

E. L. Wipfler et al.

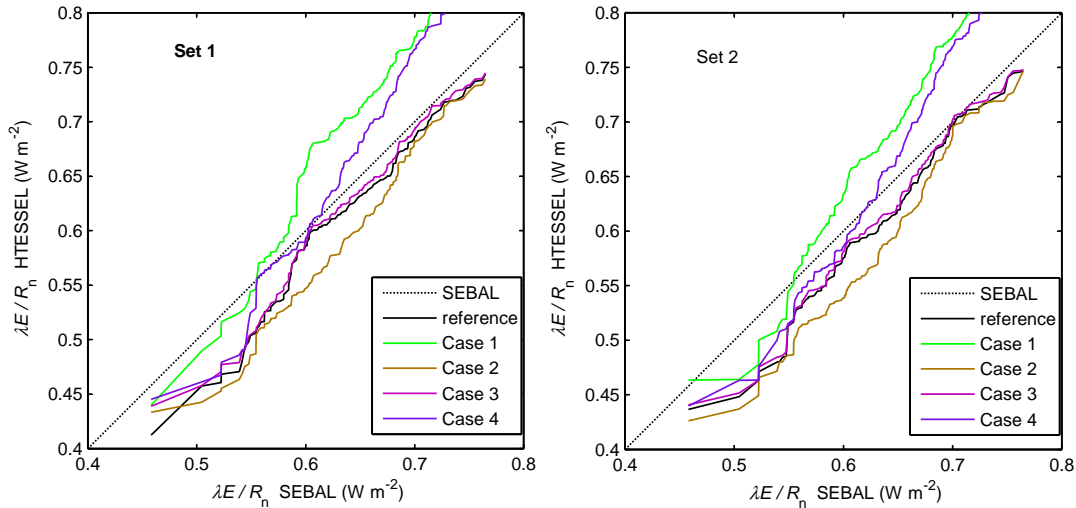


Fig. 14. Ranked SEBAL $\lambda E/R_n$ plotted against ranked HTESSEL $\lambda E/R_n$ for **(a)** initial condition Set 1 that refers to an initial soil state variable condition set and **(b)** initial condition Set 2 that refers to equilibrium of state variables over 2005.

Title Page

Abstract

Introduction

Conclusions

References

Tables

Figures

◀

▶

◀

▶

Back

Close

Full Screen / Esc

Printer-friendly Version

Interactive Discussion

